# Electromagnetic properties of the Great Pyramid: First multipole resonances and energy concentration

Mikhail Balezin,[1] Kseniia V. Baryshnikova,[1] Polina Kapitanova,[1] and Andrey B. Evlyukhin[1,2]
[1]*Department of Nanophotonics and Metamaterials, ITMO University, St. Petersburg 197101, Russia*
[2]*Laser Zentrum Hannover e.V., Hollerithallee 8, D-30419 Hannover, Germany*

(Received 21 February 2018; accepted 22 June 2018; published online 20 July 2018)

Resonant response of the Great Pyramid interacting with external electromagnetic waves of the radio frequency range (the wavelength range is 200–600 m) is theoretically investigated. With the help of numerical simulations and multipole decomposition, it is found that spectra of the extinction and scattering cross sections include resonant features associated with excitation of the Pyramid's electromagnetic dipole and quadrupole moments. Electromagnetic field distributions inside the Pyramid at the resonant conditions are demonstrated and discussed for two cases, when the Pyramid is located in a homogeneous space or on a substrate. It is revealed that the Pyramid's chambers can collect and concentrate electromagnetic energy for the both surrounding conditions. In the case of the Pyramid on the substrate, at the shorter wavelengths, the electromagnetic energy accumulates in the chambers providing local spectral maxima for electric and magnetic fields. It is shown that basically the Pyramid scatters the electromagnetic waves and focuses them into the substrate region. The spectral dependence of the focusing effect is discussed. *Published by AIP Publishing*. https://doi.org/10.1063/1.5026556

## I. INTRODUCTION

The Egyptian pyramids are one of the wonders of the world which are of great interest to people far from science as well as researchers from various scientific fields, including history, archaeology, architecture, and even physics and astronomy. Legends associated with these amazing structures excite the imagination of people engendering various fables and baseless assumptions. This is especially true of the so-called Great Pyramid—the largest and most complex from a structural point of view of the pyramids present on the plateau of Giza in Egypt.

In this context, applications of modern physical methods and approaches for investigations of Pyramids' properties are important and productive.[1–3] It could allow to make new discoveries or get new information motivating new interests to the Pyramids. For example, quite recently, cosmic-ray muon radiography was used to discover a large void (with a cross section similar to the Grand Gallery and a length of 30 m minimum) above the Grand Gallery, which constitutes the first major inner structure found in the Great Pyramid since the 19th century.[3]

In this paper, we use another modern approach and consider the Great Pyramid as a physical object that could have resonant properties when interacting with external electromagnetic waves of the radio frequency range with the corresponding wavelength $\lambda$ from 200 m to 600 m. We show that the observed resonant properties open the way to control the propagation and concentration of electromagnetic energy in the Pyramid's vicinity in this spectral range. Our investigations are based on numerical simulation of the total electromagnetic fields and total extinction and scattering cross sections[4] of the Great Pyramid using the different numerical approaches realized in CST Microwave Studio and COMSOL Multiphysics. For independent tests of our results, the method of Discrete Dipole Approximation (DDA)[5–7] is used as well. The multipole moments and the multipole decomposition of the extinction and scattering cross sections are calculated using the expressions for the Cartesian multipole moments obtained beyond the long-wavelength approximation.[4] As a result of our investigation, we find and explain a set of important features concerning the resonant concentration of electromagnetic energy by the Pyramid. Note that the method of the multipole analysis of electromagnetic wave scattering by physical objects is widely used in photonics to study the optical resonances of metal and dielectric nanoparticles.[8–10] However, this approach can be effectively used in any electromagnetic spectral range if the wavelength of an incident wave and scatter dimensions are comparable. Two of the main objectives of our study are partial removing of unreasonable speculations about electromagnetic properties of the Great Pyramid and the demonstration of flexibility of the multipole decomposition method for research at both nano- and macro-scales.

## II. THEORETICAL BACKGROUND

The interaction between the electromagnetic waves and a scattering object is basically characterized by the extinction and scattering cross sections which provide information on how much electromagnetic energy is removed from the incident beam due to its scattering and absorption. Using induced polarization $\mathbf{P}$ inside the scatterer by the incident electromagnetic wave with the complex electric field $\mathbf{E}_{inc}$, the extinction (scattering+absorption) cross section $\sigma_{ext}$ is determined by the expression[5,11]

$$\sigma_{ext} = \frac{\omega}{2W}\,\mathrm{Im}\int_V \mathbf{E}^*_{inc}(\mathbf{r})\cdot\mathbf{P}(\mathbf{r})d\mathbf{r}, \tag{1}$$

where $V$ is the volume of the scattering object, $W$ is the power of the incident wave, * denotes the complex

conjugation, and $\omega$ is the angular frequency of the incident monochromatic electromagnetic waves with the time dependence defined by $\exp(-i\omega t)$. In the case of incident electromagnetic plane waves, the power $W = (\varepsilon_0\varepsilon_d/\mu_0)^{1/2}|\mathbf{E}_{inc}|^2/2$, where $\varepsilon_0$, $\varepsilon_p$, and $\varepsilon_d$ are the vacuum dielectric constant, relative permittivities of the scatterer, and the surrounding medium, respectively, and $\mu_0$ is the vacuum permeability. Note that the induced polarization can be calculated using total electric field $\mathbf{E}$ in the scatterer $\mathbf{P} = \varepsilon_0(\varepsilon_p - \varepsilon_d)\mathbf{E}$. The scattering cross section $\sigma_{scat}$ is determined as a normalized total power scattered to the far-field zone[12]

$$\sigma_{scat} = \frac{1}{2\omega\mu_0 W}\mathrm{Im}\int_S \left[\left[\nabla\times\mathbf{E}^*_{sc}\right]\times\mathbf{E}_{sc}\right]d\mathbf{S}, \tag{2}$$

where $S$ and $d\mathbf{S}$ are the close surface around the scatterer and the surface element vector, respectively, and $\nabla$ is the nabla operator. The scattered electric field $\mathbf{E}_{sc}$ at a point $\mathbf{r}$ in the far-field zone is calculated as

$$\mathbf{E}_{sc}(\mathbf{r}) = \frac{k^2}{\varepsilon_0}\int_V \hat{G}_F(\mathbf{r},\mathbf{r}')\mathbf{P}(\mathbf{r}')d\mathbf{r}', \tag{3}$$

where $\hat{G}_F(\mathbf{r},\mathbf{r}')$ is the far-field approximation of the Green tensor corresponding to the system without the scatterer.[13,14]

Using multipole expansion of the induced polarization $\mathbf{P}$ in the irreducible representation of the Cartesian multipole moments[15] and inserting this expansion in the extinction and scattering cross sections, one can obtain their multipole presentations. The multipole contributions [up to magnetic quadrupole (MQ)] to the scattering cross section for a scatterer located in the homogeneous medium with a relative dielectric constant $\varepsilon_d$ can be written as[15]

$$\begin{aligned}\sigma_{\mathrm{sca}} \simeq{}& \frac{k_0^4}{6\pi\varepsilon_0^2|\mathbf{E}_{inc}|^2}|\mathbf{p}|^2 + \frac{k_0^4\varepsilon_d\mu_0}{6\pi\varepsilon_0|\mathbf{E}_{inc}|^2}|\mathbf{m}|^2\\ &+\frac{k_0^6\varepsilon_d}{720\pi\varepsilon_0^2|\mathbf{E}_{inc}|^2}\sum|\hat{Q}_{\alpha\beta}|^2\\ &+\frac{k_0^6\varepsilon_d^2\mu_0}{80\pi\varepsilon_0|\mathbf{E}_{inc}|^2}\sum|\hat{M}_{\alpha\beta}|^2,\end{aligned} \tag{4}$$

where $\mathbf{p}$, $\mathbf{m}$, $\hat{Q}$, and $\hat{M}$ are the electric dipole (ED), magnetic dipole (MD), electric quadrupole (EQ), and magnetic quadrupole (MQ) moments of the scatterer, respectively. The multipole presentation of the extinction cross section is given by the following formula:

$$\begin{aligned}\sigma_{\mathrm{ext}} \simeq{}& \frac{\omega}{2W}\mathrm{Im}\Big\{\mathbf{E}^*_{inc}(\mathbf{r}_0)\cdot\mathbf{p} + \mu_0\mathbf{H}^*_{inc}(\mathbf{r}_0)\cdot\mathbf{m}\\ &+\frac{1}{6}\left[\nabla\mathbf{E}^*_{inc}(\mathbf{r}_0)\right]:\hat{Q} + \frac{1}{2}\left[\nabla\mathbf{H}^*_{inc}(\mathbf{r}_0)\right]:\hat{M}\Big\},\end{aligned} \tag{5}$$

where $\nabla\mathbf{E}^*_{inc}(\mathbf{r}_0)$ and $\nabla\mathbf{H}^*_{inc}(\mathbf{r}_0)$ denote the tensors of the electric field and magnetic field gradients, respectively, and $\mathbf{r}_0$ is the position where point multipole moments are located. For the arbitrary-shaped scatterer (particle), it is convenient to take this point at the particle centre of mass.[9] The sign ":" in Eq. (5) denotes the double scalar product of tensors. Here, we use the double scalar product of two dyads $\hat{A}$ and $\hat{B}$ in the form $\hat{A}:\hat{B} = \sum_{nm}A_{nm}B_{nm}$.

In contrast to recent works[15,16] in this field, here we apply the expressions for the Cartesian multipole moments obtained beyond the long-wavelength approximation,[4] because in our consideration, the size of the scattering object is comparable to the wavelengths of indecent electromagnetic waves. With expressions for the multipole moments including the electric and magnetic dipoles and quadrupoles located at the origin of the Cartesian coordinate system, one can write as follows:[17]

$$\mathbf{p} = \int_V \mathbf{P}j_0(kr)d\mathbf{r} - \frac{k^2}{10}\int_V\left\{[\mathbf{r}\cdot\mathbf{P}]\mathbf{r} - \frac{1}{3}r^2\mathbf{P}\right\}\frac{15j_2(kr)}{k^2r^2}d\mathbf{r}, \tag{6}$$

$$\mathbf{m} = -\frac{i\omega}{2}\int_V[\mathbf{r}\times\mathbf{P}]\frac{3j_1(kr)}{kr}d\mathbf{r}, \tag{7}$$

$$\begin{aligned}\hat{Q} = {}&\int_V\left\{3(\mathbf{rP}+\mathbf{Pr}) - 2[\mathbf{r}\cdot\mathbf{P}]\hat{U}\right\}\frac{3j_1(kr)}{kr}d\mathbf{r} + 6k^2\\ &\times\int_V\left\{5\mathbf{rr}[\mathbf{r}\cdot\mathbf{P}] - (\mathbf{rP}+\mathbf{Pr})r^2 - r^2[\mathbf{r}\cdot\mathbf{P}]\hat{U}\right\}\frac{j_3(kr)}{k^3r^3}d\mathbf{r},\end{aligned} \tag{8}$$

and

$$\hat{M} = \frac{\omega}{3i}\int_V\left\{[\mathbf{r}\times\mathbf{P}]\mathbf{r} + \mathbf{r}[\mathbf{r}\times\mathbf{P}]\right\}\frac{15j_2(kr)}{k^2r^2}d\mathbf{r}, \tag{9}$$

where $j_n$ denotes the $n$-order spherical Bessel function, $\hat{U}$ is the $3\times3$ unit tensor, and $k$ is the wavenumber in the surrounding medium.

## III. PYRAMID IN HOMOGENEOUS ENVIRONMENT

To clarify the role of a pyramidal shape object on electromagnetic scattering, we first study the scattering of an external radio frequency electromagnetic wave by the Pyramid located in a homogeneous environment. The plane wave propagating along the Pyramid symmetry axis is considered for two directions (see the insets in Fig. 1). It is known that the Pyramid blocks are made of limestone. From the literature,[18–20] one can observe that the limestone permittivity value slightly varies in the range of 4–6 depending on porosity, temperature, humidity, etc. Unfortunately, we did not find the direct measured data for the permittivity dispersion of the limestone samples taken from plateau of Giza in Egypt. Therefore, we assumed that the permittivity of the Pyramid's blocks is $\varepsilon = 5 + i0.1$. Slight deviations of the permittivity from this value will only minor shift the spectrum features of the Pyramid's electromagnetic response and will not affect the obtained conclusions.

For the simulations, we use a real size 3D model of the Pyramid with the following parameters: the height of 138.75 m and each base side of 230 m. We also take the Pyramid's "King's Chamber" with the size of $11\times5\times11$ m$^3$ into the

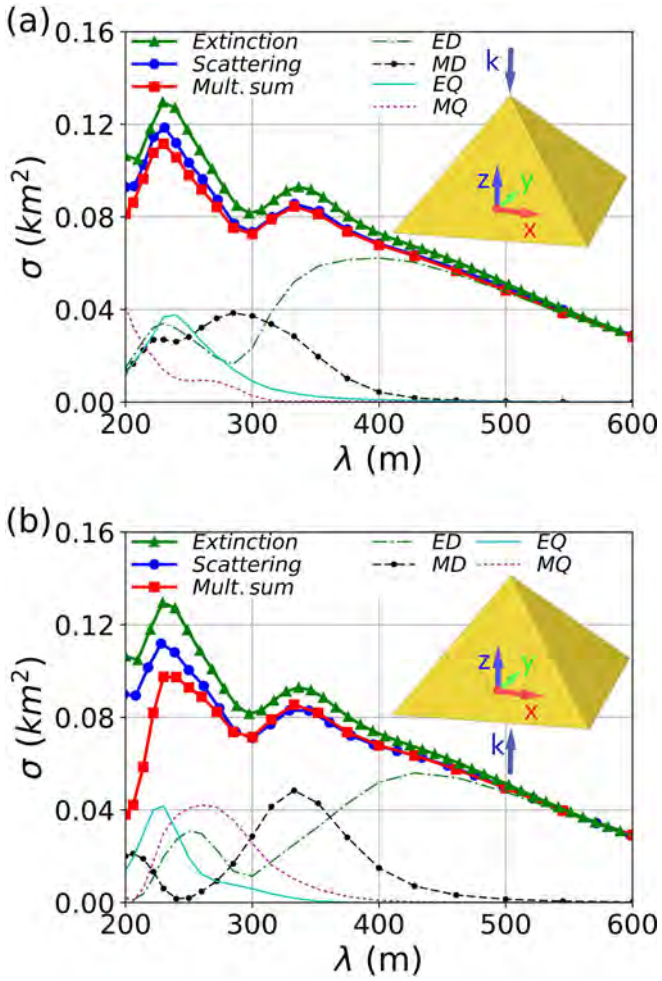


FIG. 1. Spectra of the extinction and scattering cross sections for the Pyramid located in free space and irradiated by a linear-polarized electromagnetic plane wave propagating along the vector **k** directed opposite (a) and along (b) the *z*-axis (see the insets). The electromagnetic wave is polarized along the *x*-axis.

consideration. The chamber's centre locates 5 m away from the Pyramid axis and 40.5 m higher than the Pyramid's base.

The total electric field inside the Pyramid was calculated using both CST Microwave Studio and COMSOL Multiphysics independently. From the obtained results, the spectra of the extinction and scattering cross sections and corresponding mutipole decompositions of the scattering cross sections were calculated for the two propagation directions of the incident electromagnetic waves (see Fig. 1). As soon as the spectra and corresponding mutipole decompositions obtained from the CST Microwave Studio and COMSOL Multiphysics are identical to each other, we plot only the data obtained from the CST Microwave Studio. The extinction spectra obtained by DDA are also completely consistent with results of CST Microwave Studio and COMSOL Multiphysics. For both cases of the plane wave propagation directions, the spectra demonstrate two resonant maximums at the wavelengths of $\lambda \sim 333$ m and $\lambda \sim 230$ m. Moreover, the extinction cross sections are identical for the both propagation directions of the external electromagnetic waves. The separate multipole contributions and their common contributions demonstrate that the scattering cross sections of the Pyramid are basically determined by the overlap between ED, MD, EQ, and MQ multipoles resonantly excited by the external waves. The first resonance at $\lambda \sim 333$ m is determined by ED and MD contributions, and the second one at $\lambda \sim 230$ m includes contributions of the all considered multipoles. Interestingly, relative multipole contributions into the scattering maximums of the total scattering cross section are depended on the incident direction of the electromagnetic waves. For the case presented in Fig. 1(b), the resonant peaks of the magnetic-type multipoles (MD and MQ) are shifted to the longer wavelengths compared with the case in Fig. 1(a). As a result, there are stronger resonant contributions of MD moment into the first scattering peak at $\lambda \sim 333$ m and MQ moment into the second scattering peak at $\lambda \sim 230$ m for the case when external electromagnetic waves are incident from the side of the Pyramid's base. The overlapping multipole contributions into the electromagnetic resonant scattering of the Pyramid can be explained by complex distribution of the electromagnetic fields in its volume.

Thus, we further analyse the distributions of the electric and magnetic fields in the Pyramid's volume. Figures 2 and 3 present the fields obtained by CST Microwave Studio simulations. Here (and later in this paper), we consider the electric field component of the incident wave, being equal to 1 V/m, and demonstrate the absolute values of the magnetic and electric fields in mA/m and V/m, respectively. Let us first consider the case corresponding to the incident conditions shown in Fig. 1(a). From Figs. 2(a), 2(e) and Figs. 2(b), 2(f) obtained for $\lambda = 333$ m and $\lambda = 285$ m, respectively, one can observe that in the spectral region, where the basic contribution into the scattering is done by resonant MD and ED moments of the Pyramid, the magnetic (electric) fields are concentrated at the Pyramid's centre (boundaries). With decreasing of the incident wavelength up to $\lambda = 230$ m and $\lambda = 200$ m [Figs. 2(c), 2(g) and Figs. 2(d), 2(h)], the electric (magnetic) field maximums are shifted to the Pyramid's centre (boundaries) providing strong electric field accumulation in the King's Chamber. The split of the magnetic field maximum at short wavelengths [Figs. 2(g) and 2(h)] corresponds to MQ moment excitation. In general, complex inhomogeneous distribution of electromagnetic fields for shorter wavelengths leads to overlapping of resonantly excited dipole and quadrupole multipoles. Note that the magnetic field accumulation is not observed in the King's Chamber for the all considered spectral range [Figs. 2(e) and 2(f)].

Regardless that the total extinction cross sections shown in Fig. 1 do not depend on the incident conditions, the electromagnetic field distributions inside the Pyramid are different for the same wavelengths. As a result, the different multipole decompositions for the both incident conditions are obtained. If external electromagnetic waves fall from the base side of the Pyramid [as shown in Fig. 1(b)], the electric field concentrates basically in the apex region of the Pyramid [Figs. 3(a)–3(d)] for all wavelengths. In these cases, the accumulation of the electric field in the King's Chamber is not observed. The magnetic field concentrates in the central part of the Pyramid volume and shifts to the apex with the decreasing wavelength [Figs. 3(e)–3(h)]. The obtained spectral behaviour of the magnetic field provides resonant

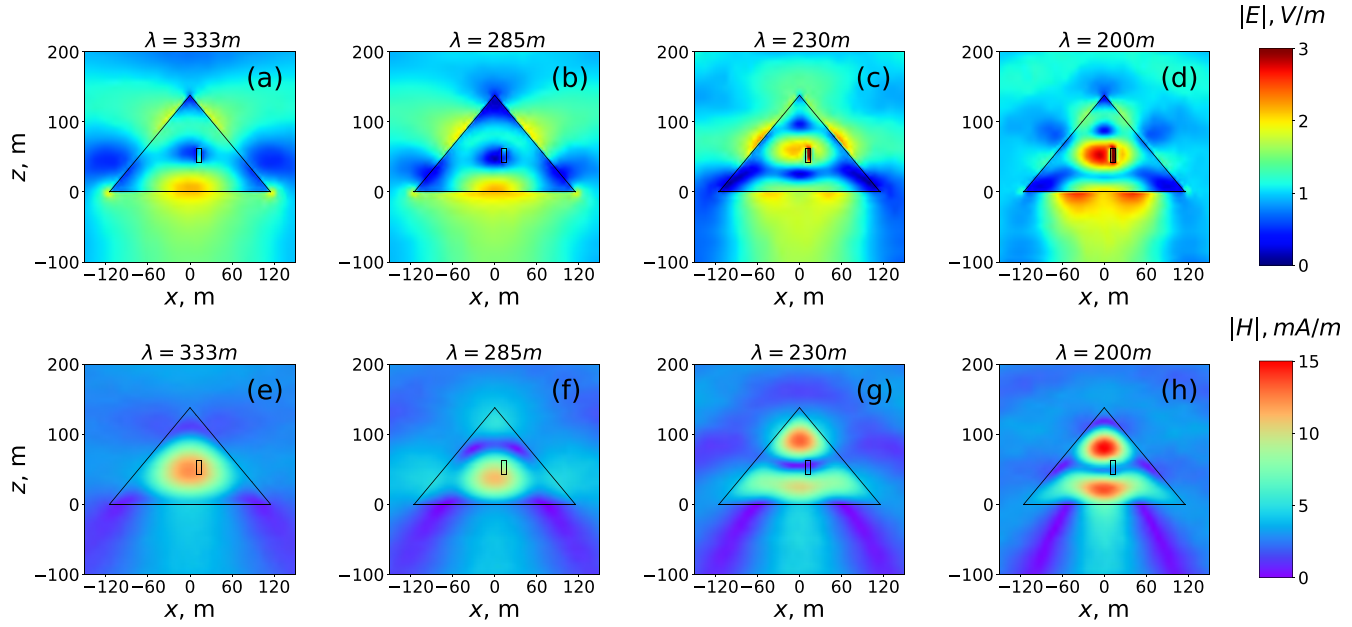


FIG. 2. Distributions of electric (a)–(d) and magnetic (e)–(h) field magnitudes in the $x$-$z$ plane of the Pyramid located in the free space. The propagation direction of the incident plane waves corresponds to Fig. 1(a). The incident waves are polarized along the $x$-axis. The black rectangular inside the Pyramid represents the "King's Chamber."

excitation of MD and MQ moments, maximums of which are shifted to the longer wavelengths as comparison with the case of the inverse incident condition. The maxima of the electric and magnetic fields intensities in the King's chamber for the both cases of propagation directions are summarized in Fig. 4.

## IV. PYRAMID ON SUBSTRATE

Next, we study the more realistic case when the Pyramid is located on the limestone plateau (substrate) as depicted in Fig. 5(a). The same value of $\varepsilon = 5 + i0.1$ is used to take into account the substrate permittivity. We consider the incident plane electromagnetic waves propagating normally with respect to the substrate surface along the vector **k** as shown in Fig. 5(a). We now take all three chambers: the "King Chamber," the "Queen's Chamber," and the chamber located under the Pyramid into the consideration. The "Queen's Chamber" is 5 m × 5 m × 6 m in size, and its centre is located at a distance of 2.5 m from the Pyramid's axis on the height of 20.8 m from the Pyramid's base. The chamber located under the Pyramid has the size of 5.2 m × 5.6 m × 4.6 m. Its centre is moved from the Pyramid's axis on

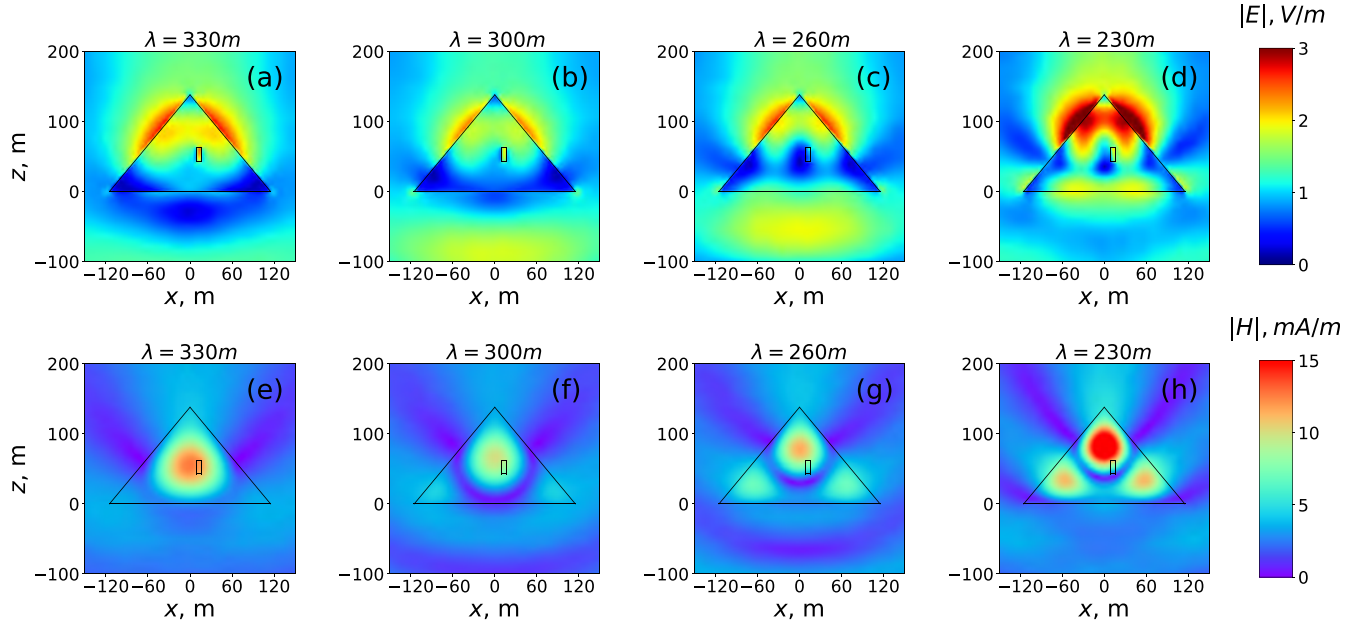


FIG. 3. Distributions of electric (a)–(d) and magnetic (e)–(h) field magnitudes in the $x$-$z$ plane of the Pyramid located in the free space. The propagation direction of the incident plane waves corresponds to Fig. 1(b). The incident waves are polarized along the $x$-axis. The black rectangular inside the Pyramid represents the "King's Chamber."

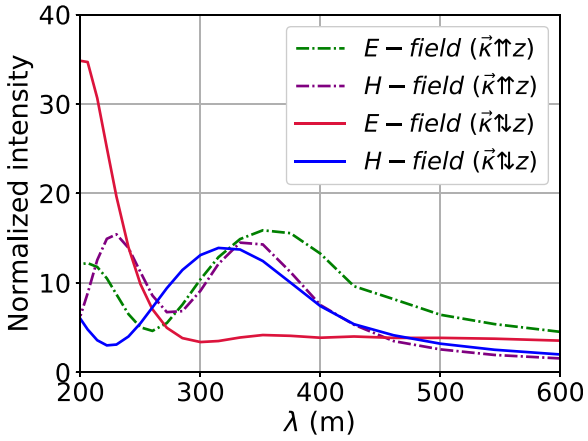


FIG. 4. Spectra of the maximum values of the normalized electric and magnetic field intensities in the King's chamber of the Pyramid for both directions of the incident wave propagation. The fields are normalized on the corresponding intensities of the incident waves.

2.4 m and situated at a distance of 29.8 m below the Pyramid's base.

Spectra of the extinction cross section and its multipole decomposition are presented in Fig. 5(b). In the considered wavelength range, the extinction cross section has only one broad maximum at $\lambda \sim 250$ m. This maximum is a result of the overlap between all considered multipoles, especially the contributions corresponding to ED, MD, and MQ moments. [Note that in Fig. 5(b), we also calculated the contribution from the electric octupole (EO) moment.] One can expect that the strong magnetic field will be concentrated inside the Pyramid at this spectral range. It is important to mention that the small imaginary part of limestone permittivity leads to weak absorption of the electromagnetic energy by the Pyramid. Thus, the extinction cross section is basically determined by the electromagnetic scattering.

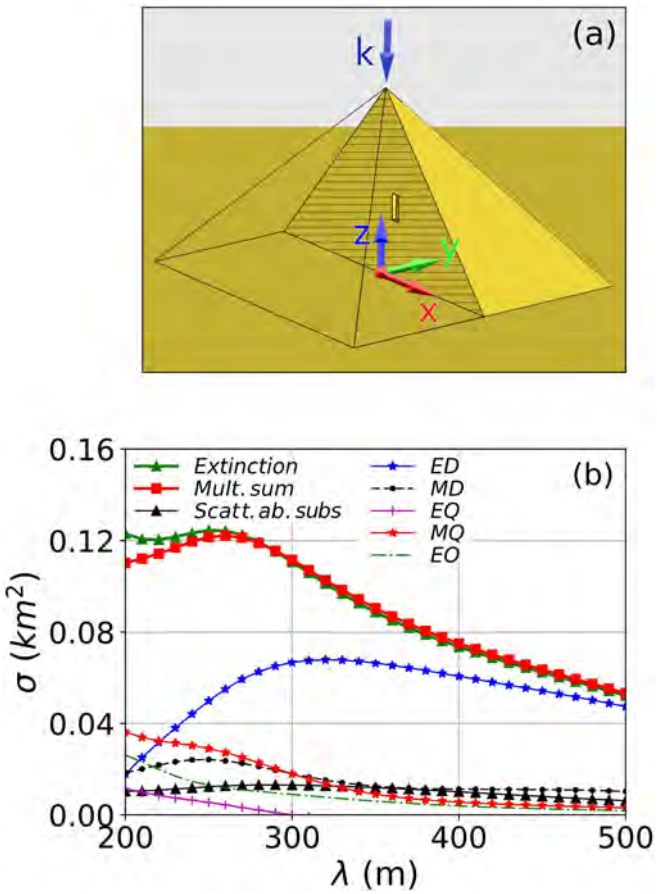


FIG. 5. (a) Schematic representation of the Pyramid located on a substrate. The electromagnetic linear-polarized (along the $x$-axis) plane wave propagates along the vector **k**. (b) Spectra of the extinction and scattering cross sections for the Pyramid located on the substrate. Contributions provided by the main multiples are shown as well.

In Fig. 5(b), we also demonstrate the partial scattering cross section corresponding to the scattering only above the substrate by a black triangle curve. Comparing it to the total extinction cross section, one can observe that most part of scattered electromagnetic energy propagates into the substrate. To demonstrate it, we plot the distribution of electric and magnetic fields in the simulated volume in Fig. 6. It is clearly seen that most of the electromagnetic energy leaves the Pyramid and focuses directly under its base. At a shorter wavelength, the focusing effect increases due to resonant excitation of the Pyramid's multipole moments. Note that the maxima of the electric and magnetic fields are located just under the Pyramid's basis in the region of the third chamber. This effect is especially strong for the magnetic field as shown in Figs. 6(f)–6(j).

Another important observation we did is the concentration of electromagnetic fields inside the Pyramid and especially inside its chambers (see Fig. 7). As an example, we plot the magnitude of electric field distribution inside the Pyramid and its chambers at the wavelength $\lambda = 200$ m in Fig. 7(a). The intensities of electric and magnetic fields have been calculated inside the chambers over the spectral range of interest. The maximal values of electromagnetic field intensities inside the chambers are shown in Figs. 7(b)–7(d). At the shorter wavelengths, the field intensities increase in comparison to the longer wavelengths. It can be explained by the excitation of the Pyramid's higher-order multipoles which are characterized by the non-uniform electromagnetic field distributions, resulting in higher energy density inside the Pyramid. Interestingly, to note that the accumulation of the electromagnetic energy in the chamber under the Pyramid is realized in the electromagnetic focusing region [see Figs. 7(a) and 7(d)].

## V. CONCLUSION

In this study, we have considered electromagnetic excitation of the Great Pyramid by plane waves with the wavelengths being larger than the typical size of the scatterer. In this case, only several first-order multipole resonances have been observed. The multipole analysis of electromagnetic wave scattering by the Great Pyramid has been performed in the radio frequency range and revealed important physical properties concerning the accumulation and focusing of electromagnetic energy. It has been shown that the Pyramid can resonantly scatter electromagnetic waves and support resonant excitation of electromagnetic multipoles which resulted from strong electromagnetic fields in the Pyramid volume. For the Pyramid located in the free space, we have demonstrated that

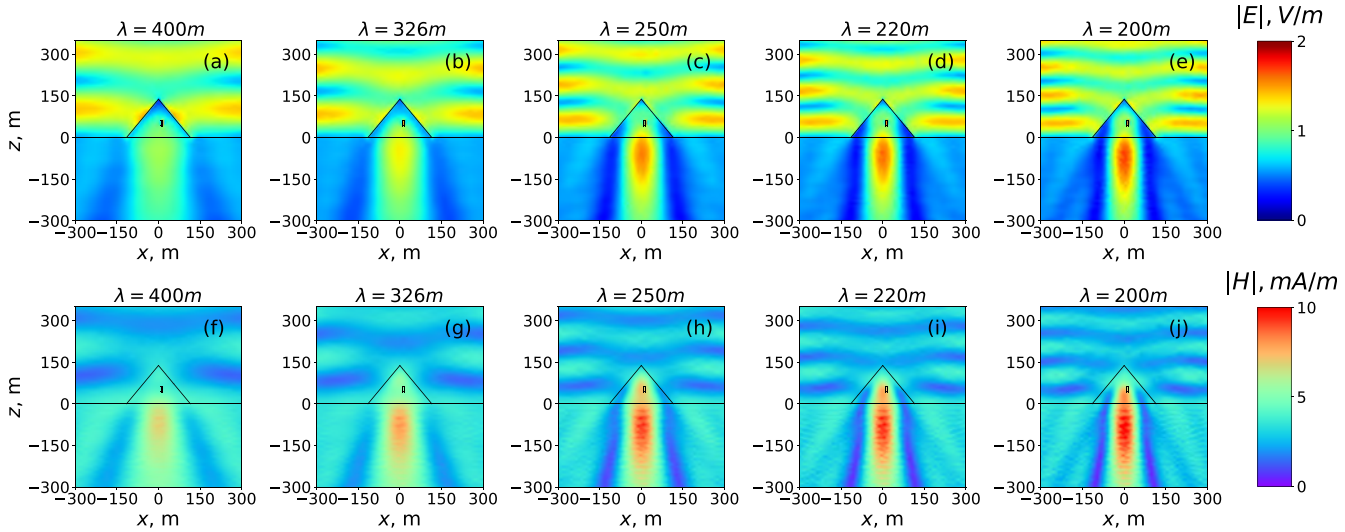


FIG. 6. Distributions of electric (a)–(e) and magnetic (f)–(j) field magnitude in the *x*-*z* plane of the Pyramid and its supporting substrate. The propagation direction of the incident plane waves corresponds to Fig. 5. The polarization of the incident waves is along the *x*-axis. The black rectangular inside the Pyramid represents the position of the "King's Chamber."

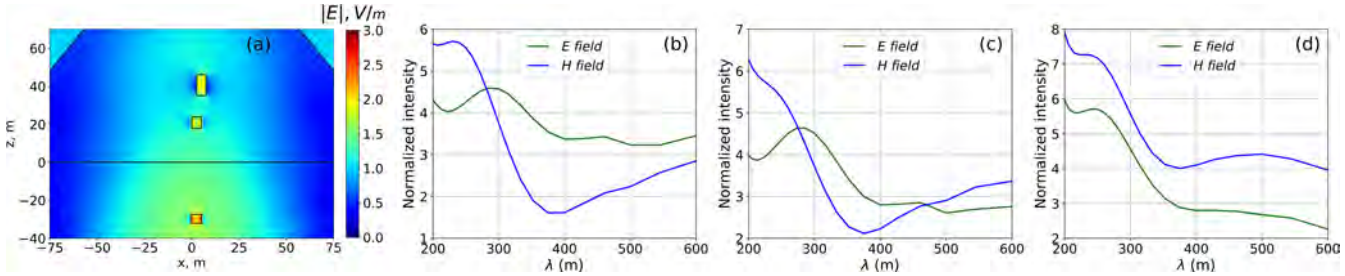


FIG. 7. (a) Distribution of electric field magnitude inside the Pyramid, including its chambers at the wavelength $\lambda = 200$ m. Field scale, configuration, and incident wave conditions correspond to Fig. 6. Spectra of maximal values of the normalized electric and magnetic field intensities in the Pyramid's chambers: (b) "King's chamber"; (c) "Queen's chamber"; (d) chamber under the Pyramid. The lines are obtained by an approximation of the calculated fields for discrete values of incident wavelengths. The field intensities are normalized on the corresponding intensities of the incident waves.

the total extinction cross-section does not depend on the considered incident conditions; however, the electromagnetic field distributions inside the Pyramid are different for the same wavelengths. It leads to the different multipole decompositions for the both considered incident conditions. For the Pyramid located on the substrate, we found that it basically scatters electromagnetic waves into the substrate, where the focusing effect is observed. It was established that the Pyramid's chambers can concentrate electromagnetic energy at the resonant conditions. In general, one may conclude that pyramidal objects located on a substrate and supporting multipole resonances can significantly suppress the reflection of incident electromagnetic waves. In the earth conditions, this could be used for controlling the radio-wave propagation and reflection. Due to the scaling properties, such a behaviour can be realized in different spectral ranges for suitable material and geometrical parameters.

The obtained results can be considered as a first step to the further investigation of the Great Pyramid electromagnetic properties. This approach can be extended to other physical objects and geometries. As an example, one can now study the complex system of the pyramids located at the Giza plateau.

In the conclusion, note that the excitation of the Pyramid with shorter incident wavelengths, than considered here, could result in the excitation of higher order resonances with strong field concentration effects. But it is out of the scope of the current work and will be a next step of our investigations.

## ACKNOWLEDGMENTS

The results of numerical simulation by CST Microwave Studio were supported by Russian Science Foundation, Project No. 17-79-20379. DDA modelling was supported by Russian Science Foundation, Project No. 16-12-10287. The financial support from the Deutsche Forschungsgemeinschaft (DFG), Project No. EV 220/2-1, is acknowledged.

[1]L. W. Alvarez, J. A. Anderson, F. E. Bedwe *et al.*, "Search for hidden chambers in the pyramids," Science **167**, 832–839 (1970).
[2]K. Morishima, A. Nishio, M. Moto, T. Nakano, and M. Nakamura, "Development of nuclear emulsion for muography," Ann. Geophys. **60**, S0112 (2017).
[3]K. Morishima, M. Kuno, A. Nishio *et al.*, "Discovery of a big void in Khufu's Pyramid by observation of cosmic-ray muons," Nature **552**, 386–390 (2017).
[4]R. Alaee, C. Rockstuhl, and I. Fernandez-Corbaton, "An electromagnetic multipole expansion beyond the long-wavelength approximation," Opt. Commun. **407**, 17–21 (2018).

[5]B. T. Draine, "The discrete-dipole approximation and its application to interstellar graphite grains," Astrophys. J. **333**, 848 (1988).
[6]A. B. Evlyukhin, C. Reinhardt, E. Evlyukhin, and B. N. Chichkov, "Multipole analysis of light scattering by arbitrary-shaped nanoparticles on a plane surface," J. Opt. Soc. Am. B **30**, 2589 (2013).
[7]M. A. Yurkin and A. G. Hoekstra, "The discrete dipole approximation: An overview and recent developments," J. Quant. Spectrosc. Radiat. Transfer **106**, 558 (2007).
[8]P. D. Terekhov, K. V. Baryshnikova, Y. A. Artemyev, A. Karabchevsky, A. S. Shalin, and A. B. Evlyukhin, "Multipolar response of nonspherical silicon nanoparticles in the visible and near-infrared spectral ranges," Phys. Rev. B **96**, 035443 (2017).
[9]A. B. Evlyukhin, C. Reinhardt, and B. N. Chichkov, "Multipole light scattering by nonspherical nanoparticles in the discrete dipole approximation," Phys. Rev. B **84**, 235429 (2011).
[10]D. Sikdar, W. Cheng, and M. Premaratne, "Optically resonant magneto-electric cubic nanoantennas for ultra-directional light scattering," J. Appl. Phys. **117**, 083101 (2015).
[11]T. Søndergaard and S. I. Bozhevolnyi, "Surface plasmon polariton scattering by a small particle placed near a metal surface: An analytical study," Phys. Rev. B **69**, 045422 (2004).
[12]L. Novotny, "Allowed and forbidden light in near-field optics. II. Interacting dipolar particles," J. Opt. Soc. Am. A **14**, 105 (1997).
[13]L. Novotny, B. Hecht, and D. Pohl, "Interference of locally excited surface plasmons," J. Appl. Phys. **81**, 1798 (1997).
[14]L. Novotny and B. Hecht, *Principles of Nano-Optics* (Cambridge University, New York, 2006).
[15]A. B. Evlyukhin, T. Fischer, C. Reinhardt, and B. N. Chichkov, "Optical theorem and multipole scattering of light by arbitrarily shaped nanoparticles," Phys. Rev. B **94**, 205434 (2016).
[16]P. D. Terekhov, K. V. Baryshnikova, A. S. Shalin, A. Karabchevsky, and A. B. Evlyukhin, "Resonant forward scattering of light by high-refractive-index dielectric nanoparticles with toroidal dipole contribution," Opt. Lett. **42**, 835–838 (2017).
[17]V. A. Zenin, A. B. Evlyukhin, S. M. Novikov, Y. Yang, R. Malureanu, A. V. Lavrinenko, B. N. Chichkov, and S. I. Bozhevolnyi, "Direct amplitude-phase near-field observation of higher-order anapole states," Nano Lett. **17**, 7152–7159 (2017).
[18]J. L. Davis and A. P. Annan, "Ground-penetrating radar for high-resolution mapping of soil and rock stratigraphy," Geophys. Prospect. **37**, 531–551 (1989).
[19]A. Martinez and A. P. Byrnes, "Modeling dielectric-constant values of geologic materials: An aid to ground-penetrating radar data collection and interpretation," Curr. Res. Earth Sci. **247**, 1–16 (2002).
[20]S. O. Nelson, "Determining dielectric properties of coal and limestone by measurements on pulverized samples," J. Microwave Power Electromagn. Energy **31**, 215–220 (1996).